

# Numerical Paleoceanographic Study of the Early Jurassic Transcontinental Laurasian Seaway

Christian J. Bjerrum<sup>1</sup>, and Finn Surlyk

Geological Institute, University of Copenhagen, Copenhagen, Denmark

John H. Callomon

Chemistry Department, University College London, London, England, United Kingdom

Rudy L. Slingerland

Department of Geosciences, Pennsylvania State University, University Park, Pennsylvania

**Abstract.** The forces governing marine circulation of a meridional transcontinental seaway is explored with the Princeton Ocean Model. The Jurassic Lurasian Seaway, which connected the low-latitude Tethys Ocean with the Arctic Sea is modeled quantitatively. The global ocean is found to have a profound influence on seaway dynamics. A north-south density difference and hence sea level difference of the global ocean was probably the main factor in forcing the seaway flow. When the Tethys waters were the denser water, the net seaway flow was southward, and conversely, it was northward for denser Arctic waters. Marine bioprovincial boundaries and sediment data indicate that the seaway probably was dominated by Boreal faunal groups and reduced salinities several times in the Jurassic. The model results suggest that this can be explained by southward flowing seaway currents, which may have been related to an oceanic thermohaline circulation where no northern high-latitude deep convection occurred.

## 1. Introduction

Transcontinental seaways connecting tropical oceans with northern high-latitude oceans have existed repeatedly through geological time [Smith *et al.*, 1994]. However, their marine dynamics remain poorly understood because of a lack of modern analogues. Only the Cretaceous Western Interior Seaway of North America has been modeled in any detail, and the conclusions have been contradictory [Erickson and Slingerland, 1990; Jewell, 1996; Slingerland *et al.*, 1996]. Slingerland *et al.* [1996] deduced that the circulation was anticyclonic, whereas Jewell [1996] concluded it was cyclonic. If straits connecting present-day ocean basins may be regarded as small-scale analogues of transcontinental seaways (e.g., the Bering Strait or the straits around Japan), then their flow dynamics on the annual mean should be governed by density differences in the upper water columns and hence by the hydrostatic sea level difference between the oceans on either side [e.g., Gill, 1982; Stigebrandt, 1984; Ohshima, 1994; Shaffer and Bendtsen, 1994]. The hydrostatic sea level difference is derived from the depth-integrated hydrostatic

pressure difference along with an assumption of a level of no motion at a fixed depth below the permanent thermocline [e.g., Stigebrandt, 1984]. The resulting mean unidirectional barotropic flow is different from two-way strait flow because the oceanic level of no motion lies deeper than the strait bottom [Whitehead, 1998; Hay, 1995]. In some present-day straits the sea level difference results in a mean barotropic flow, but it remains to be demonstrated whether these results can be extended to ancient transcontinental seaways.

The aim of the present study is to increase the understanding of marine dynamics of latitude-spanning transcontinental seaways. Focus is placed on the relatively shallow transcontinental Lurasian Seaway [e.g., Ziegler, 1990] (Figure 1). The Lurasian Seaway is here defined to be the transcontinental sum of interconnected Jurassic straits and seas between the northern margin of the Tethys Ocean and the Boreal Arctic Sea north of the pre-North Atlantic region and Europe. The seaway is important because its deposits constrain much of our current knowledge of the Jurassic-Early Cretaceous climate and because it records the initial opening of the North Atlantic. Understanding of the nature and origin of economically important Lower and Upper Jurassic hydrocarbon source rocks may also be obtained by investigating the seaway paleoceanography. The Lurasian Seaway differs from the Cretaceous Western Interior Seaway of North America in that it probably was shallower and contained many islands. Further, the Arctic connection to the paleo-Pacific was much wider than the Western Interior

<sup>1</sup>Now at Danish Center for Earth System Science, University of Copenhagen, Copenhagen, Denmark.

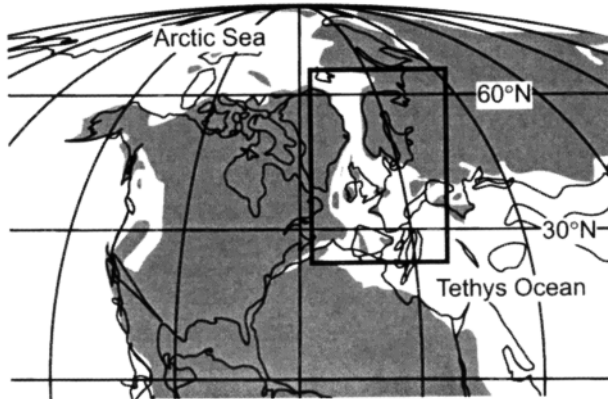


**Figure 1.** Toarcian paleogeography. The transcontinental area of interest is framed. Paleoland areas are dotted. Modified from *Smith et al.* [1994].

Seaway connection [*Smith et al.*, 1994]. Previous studies of the Laurasian Seaway circulation were qualitative and based on the distribution of sediments and fauna. *Ager* [1975] proposed that the subtropical influence of the Tethys extended northward over the epicontinental shelf in southern Europe and that seaway currents originating in the Arctic to a variable degree influenced northern Europe. The generally Boreal nature of the fauna of northern Europe suggests that the region at times was characterized by reduced salinities and that boreal sea currents probably flowed southward into the region of the North Sea [*Hallam*, 1969; *Ager*, 1975]. The southward movement of boreal faunas and the north-south trends in authigenic uranium content suggest a similar situation for the Late Jurassic [*Miller*, 1990]. The more precise nature and ultimate cause of these currents remain to be understood.

Here we explore the circulation dynamics of the Early Jurassic Laurasian Seaway during times of high relative sea level using the Princeton Ocean Model (POM) [*Blumberg and Mellor*, 1987; *Mellor*, 1998]. The successful application of POM to present ocean circulation lends some confidence to the use of POM in paleoceanographic studies provided the boundary conditions (BC) are correct, i.e., bathymetry, surface, and open-boundary forcing. Because the boundary conditions are poorly constrained for the geological past, the POM is here used in a process study. The origin and nature of the large-scale current patterns are determined from a series of numerical model calculations that are constrained by the annual mean surface forcing as diagnosed from the atmospheric general circulation model (AGCM) calculations of *Chandler et al.* [1992]. The relative importance of wind, inflow/outflow, and buoyancy forcing fields in driving the circulation is investigated, as is the sensitivity of circulation and water characteristics in the absence of a hydrostatic sea level difference and various conjectured bathymetries. Our results demonstrate that a north-south density difference and resulting hydrostatic sea level difference is likely to have been the

main factor controlling the mean flow in this transcontinental seaway.

## 2. Geological Setting

During times of high relative sea level in the late Early Jurassic (Toarcian), Europe and the North Atlantic regions were characterized by an extensive system of straits and seas extending from an Arctic Sea north of 60°N to the Tethys Ocean south of 30°N paleolatitude [*Hallam*, 1988; *Ziegler*, 1990; *Smith et al.*, 1994], in which faunal extinctions, deposition of highly kerogen-rich shales, and isotopic excursions occurred [*Jenkyns*, 1988; *Hesselbo et al.*, 2000; *Hallam and Wignall*, 1997]. *Hallam* [1984, 1993] reviewed the lithofacies and faunal distributions in the Jurassic “greenhouse” world and found that northwest Europe was probably warm and humid during the Early Jurassic. The sea surface temperatures have been hypothesized to have ranged from 26°C in the south to 5°–10°C in the north in agreement with coral and paleobotanical data [e.g., *Hallam*, 1969; *Chandler*, 1994; *Rees et al.*, 2000].

The salinity in the south was most likely close to normal, whereas farther north the salinity might have been reduced by up to 10 practical salinity units (psu) [*Hallam*, 1969; *Prauss et al.*, 1991; *Sælen et al.*, 1998]. The presence of Toarcian black organic-rich shales, in part laminated, indicates that the central to southeastern part of seaway must have had highly productive surface waters and/or anoxic bottom waters [*Jenkyns*, 1988; *Röhl et al.*, 2001; *Schouten et al.*, 2000].

## 3. Model and Formulation of BC

The numerical development of the POM is given in *Blumberg and Mellor* [1983, 1987] and *Mellor* [1998] ([www.aos.princeton.edu/WWWPUBLIC/htdocs.pom](http://www.aos.princeton.edu/WWWPUBLIC/htdocs.pom)). A detailed treatment of the governing equations and the formulation of the BC as used in the present study is given by *Oey and Chen* [1992]. Formulations of the numerical BC are described below. Assumptions about poorly constrained values are presented in section 4.

### 3.1. Surface Boundary Conditions

At the free surface in the model the annual mean wind stress vector components are modulated by an oscillatory component [*Blumberg and Mellor*, 1983]. This modulation is a crude approximation to synoptic storms giving a more realistic mixed layer depth. The sea surface temperature  $T$  is restored to a prescribed temperature  $T_c$  [*Cai and Godfrey*, 1995].  $T_c$  refers to prescribed external values that are essentially unknown and here taken from an AGCM [*Chandler et al.*, 1992]. A linear restoring time of 60 days for the top 30 m of water is used for restoring  $T$  to  $T_c$ . Using a restoring BC on  $T$  allows  $T$  to be influenced by the advection of heat and deviate from  $T_c$ . A constant salinity flux is calcu-

lated from the precipitation minus open water evaporation rate ( $P - E_p$ ) of the AGCM.

The flux of momentum at the sea bottom is balanced by matching the computed bottom velocity with the logarithmic boundary layer formulation [Mellor, 1998]. A variable roughness  $z_r = 0.01 + 1.0/H$  (in meters), is used as a crude parameterization of the effect that shallow water waves have on modulating the roughness length scale [Oey, 1998; Holloway and Barnes, 1998]. The resulting drag coefficient varies from  $5.0 \times 10^{-3}$  at  $H = 200$  m to  $22.5 \times 10^{-3}$  in shallow water ( $H = 30$  m).

River runoff from continents is parameterized with velocities at discrete grid points [Oey, 1996]. The injected water is assumed to have a temperature of  $T_c$  and a salinity  $S = 0.2$  psu. Island runoff is parameterized with the surface salinity BC on the surrounding "wet" grid points. Half of the freshwater ( $P - E_l$ ) summed over the island is added to the  $P - E_p$  of the wet node (see below).

### 3.2. Open Ocean Boundaries

A radiation condition on open boundaries is used for the barotropic model velocities [Oey and Chen, 1992]. A Sommerfeld-type radiation condition is used for the internal baroclinic velocities. The unknown temperature profile  $T_{cp}$  and salinity profile  $S_{cp}$  are prescribed during inflow, whereas a linearized advection equation is solved during outflow [Oey and Chen, 1992; Mellor, 1998].

## 4. Bathymetry and External Forces

### 4.1. Paleogeography and Bathymetry

The Early Jurassic, Toarcian, paleogeography used as the starting point for the model calculations is based on the work of Smith *et al.* [1994], with details from Ziegler [1988, 1990, and references therein] and Bradshaw *et al.* [1992] (Figure 2). All latitude designations throughout the paper are paleolatitudes from Smith *et al.* [1994]. In principle, detailed mapping of facies and sedimentary structures can be interpreted to give good information on water depth (as by Diem [1984] and Buchem and McCave [1989]). However, the spatially and temporally fragmented rock record at places in the western part of the seaway necessitate the inexact first-order approach adapted here.

The Early Jurassic was to a large extent characterized by postrift thermal subsidence in the region, which resulted in subbasins with isopach contours that exhibit a relatively smooth "bull's-eye pattern" when post-Toarcian erosion is removed by interpolation [Ziegler, 1990]. Lithology maps from Bradshaw *et al.* [1992] and Ziegler [1988, 1990] are used to delineate deeper shelf water (>30 m, shale) and shallow water (<20-30 m, sandstone-mudstone), which in turn, is used to define a conjectured relative bathymetry.

The absolute bathymetry is constructed by combining relative water depth information with the occurrences of the common Toarcian laminated offshore shales as follows: The

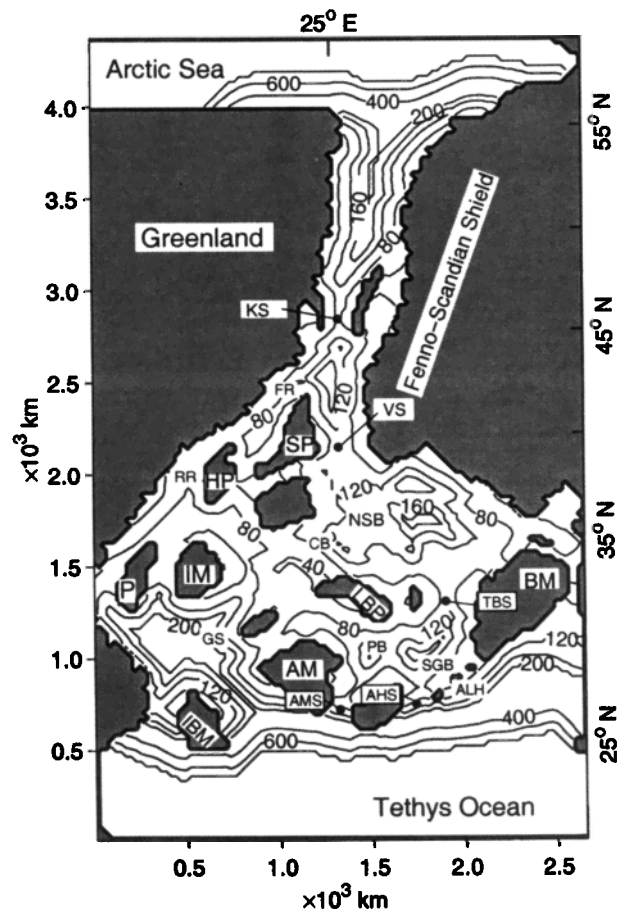


**Figure 2.** Conjectured model bathymetry for the Laurasian Seaway during maximum flooding (weakly smoothed for numerical stability). The variations in relative bathymetry are approximated from lithofacies variations shown by Ziegler [1990] (see text). Contour intervals (CI) are 40 m above 200 m depth and 200 m below. Coastline uncertainties may be as large as 200 km laterally, and bathymetric errors are of the order of 20-100 m in areas with little data. Map coordinates are paleolatitude as used throughout the text. ALH, Alemannic High; AM, Armorican Massif; BM, Bohemian Massif; HP, Hebrides Platform; IBM, Iberian Meseta; IM, Irish Massif; LBP, London-Brabant Platform; P, Porcupine Bank; SP, Shetland Platform; AHS, Alemannic High Strait; AMS, Armorican Massif Strait; CB, Cleveland Basin; FR, Faeroe Strait; KS, Koch Strait; GS, Goban Spur; NSB, North Sea Basin; PB, Paris Basin; RR, Rockall Strait; SGB, South German Basins; TBS, Thuringian-Brandenburg Strait; VS, Viking Strait.

water depth determined from the laminated shale (see below) is tapered to the approximate coastline of the paleogeography used, such that bathymetry contours parallel the smoothed relative bathymetry contours based on lithofacies. Where limited information is available, such as between Norway and Greenland, water depths were subjectively assigned, such that narrow regions between islands were assigned a sill depth of 80 m and intervening marine areas were assigned a depth of 180 m.

Offshore laminated mudstones with no indication of wave agitation could have been deposited at any water depth be-

low storm wave base. The maximum wave orbital velocities as a function of depth can be found from semiempirical relations between free fetch and storm wind speed [e.g., *Bretschneider*, 1966]. Assuming that velocities must have been  $<0.1 \text{ m s}^{-1}$  for the fine lamination not to be disturbed, the minimum water depths can be estimated. For example, given a wind fetch of 500 or 1000 km and a storm of unlimited duration with a wind speed of  $20 \text{ m s}^{-1}$ , water depths must have been  $>90$  or  $220 \text{ m}$ , respectively, during deposition of laminated offshore shales. A maximum water depth of  $200 \text{ m}$  has been used in the model at locations of laminated shales and a large free fetch (Figure 2). This estimate is the same as other estimates of depth for comparable offshore facies of Late Jurassic age in southern Europe [*Picard et al.*, 1998]. The Toarcian finely laminated shales alternate with wavy to crinkly laminae, where the latter may be indicative of stabilization by microbial mats [*O'Brian*, 1990; *Schieber*, 1999]. The stabilization would have resulted in a 75-200% increase in the critical shear velocity necessary to mobilize sediments [*Paterson and Black*, 1999]. However, the finely laminated shales were probably deposited without the involvement of microbial mats [*O'Brian*, 1990; *Schieber*, 1999]. Model sensitivity tests further show that the results are fairly robust to a 50% reduction in bathymetry.

The conjectured Early Jurassic model bathymetry ranges from 30-200 m in the seaway down to 750 m in the basins north and south of the seaway (Figure 2). Model depths of 30-50 m are used along most coastlines in the absence of better data. Tidal amplification and associated residual currents, such as occur at depths shallower than 50 m in the North Sea and English Channel, can therefore not be modeled here and will be treated in a future study.

The name Viking Strait (VS) is used here to refer to the Viking Graben and northernmost North Sea areas (Figure 2). This usage is more restricted compared to previous usage [*Callomon*, 1979]. The Koch Strait (KS) is here used for the narrow region at  $46^\circ\text{N}$  paleolatitude between the West Haltenbanken Highs (offshore mid-Norway) and East Greenland. Thus, the Koch Strait refers to the marine connection over the area that has been called the East Greenland Shelf Basin and Møre-Vøring Basin Trend [*Dreyer*, 1992]. The Arctic and Tethys Basins are highly simplified and are included only to move the open boundaries of the model away from the area of interest.

It should be emphasized that local paleobathymetry details and interpretations by other authors may differ substantially from the map used here. In certain areas uncertainties in the coastal reconstruction are up to 200 km and potential errors in bathymetry are of the order of 50-100 m. The map is taken as a necessary first-order starting point in order to identify the physical processes operating in the seaway at scales larger than individual subbasins. The importance of errors in the assumed bathymetry is tested in model calculations by varying this parameter (section 7).

A transverse Mercator projection of the reconstructed Early Jurassic seaway is mapped onto a Cartesian computa-

tional grid with a 27 km resolution ( $101 \times 165$  grid points). The initially conjectured bathymetry is weakly smoothed before the model calculations [*Mellor*, 1998]. Vertically, 13 grid points are used, closely spaced near the surface and at intermediate resolution near the bottom. Model calculations are done with a time step of 80 s for the barotropic mode and 2000 s for the baroclinic mode.

## 4.2. External Prescribed Forces

The external forcing imposed on the model through the surface boundary conditions are wind stress, surface heat flux, net freshwater flux (precipitation minus evaporation), and river runoff. All these quantities are essentially unknown for the Jurassic but are here taken from atmospheric general circulation model calculations. Additionally, external vertical salinity and temperature profiles at the open boundaries (OBC) impose important buoyancy forces north and south of the seaway.

**4.2.1. Surface forcing.** The surface boundary conditions are computed from the AGCM of *Chandler et al.* [1992]. M. A. Chandler provided the annual average data files from the Early Jurassic AGCM calculations. Other Jurassic AGCM's have been published in detail [*Valdes and Sellwood*, 1992; *Moore et al.*, 1992]. The results of *Valdes and Sellwood* [1992] were for the Late Jurassic time interval and did not include open water in the region of the seaway. The wind field results of *Moore et al.* [1992] are here used in a sensitivity test. The remaining forcing fields from *Moore et al.* [1992] are not available in digital format and could therefore not be used.

The AGCM annual average wind stress field has weak westerly winds north of  $50^\circ\text{N}$  (stress  $< 0.03 \text{ N m}^{-2}$ , Figure 3). Subtropical northeasterly trade winds characterize the southern domain of the model and have a maximum wind stress of  $0.05 \text{ N m}^{-2}$ , which is  $0.01\text{-}0.04 \text{ N m}^{-2}$  less than today. Northwesterly winds are present over the western part of the seaway at  $35^\circ\text{N}$ .

The surface temperature  $T_c$  used in calculating the model sea is the same as the lower AGCM "forcing" boundary condition used by *Chandler et al.* [1992].  $T_c$  decreases almost linearly from  $28^\circ\text{C}$  at  $20^\circ\text{N}$  to  $12^\circ\text{C}$  at  $60^\circ\text{N}$ .

The freshwater annual average of precipitation minus open-water evaporation ( $P - E_p$ ) of the AGCM is zonally averaged over the seaway (Figure 4). South of  $40^\circ\text{N}$ , open water experiences net evaporation, whereas excess net precipitation dominates farther north. The magnitudes of  $P - E_p$  are comparable with open oceanic conditions today, but the minimum is displaced  $5^\circ\text{-}10^\circ$  northward, whereas the maximum is displaced  $10^\circ$  southward [*Silva et al.*, 1994].

**4.2.2. Rivers.** Mainland river runoff is assumed to come from 30 geographically evenly distributed rivers along the seaway margins. The river volume transport is calculated from the terrestrial  $P - E_l$  over the designated drainage areas, assuming a 50% drainage efficiency [*Holland*, 1978; *Jewell*, 1996]. The drainage surfaces are assumed to be five

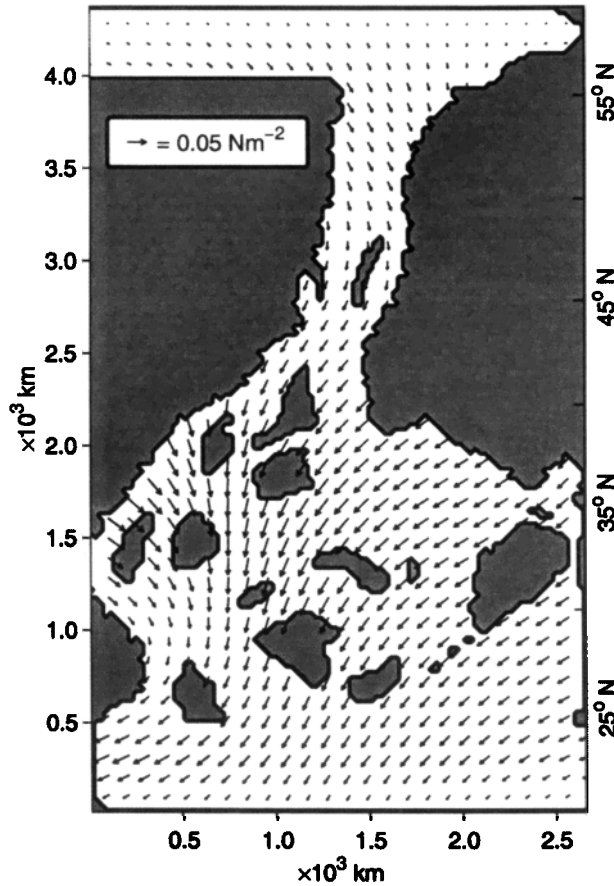


**Figure 3.** Surface wind stress vectors obtained from the AGCM of Chandler *et al.* [1992] after spline interpolation. Maximum stress is over the North Sea region. Northeasterly trade winds dominate most of the southern and eastern seaway. Weak westerlies are present north of 45°N.

grid points wide (north-south) and to extend 500 km inland from the seaway margin. The seaway circulation is found not to be very sensitive to uncertainties in drainage areas and efficiency.  $P - E_l$  is found by the empirical Thornthwaite relation, where evapotranspiration  $E_l$  is calculated from the AGCM surface air temperature and hours of daylight and  $P$  is the AGCM zonally averaged precipitation over the seaway (Figure 4) [Chandler, 1994].

**4.2.3. Open boundary conditions and external elevation.** The Arctic and Tethys Basins are taken to have open boundaries to the west and east, respectively. The external elevation difference between Arctic and Tethys sea surface imposed on the boundaries is found at each time step from the hydrostatic sea level difference  $\Delta\eta$  using the density-depth profiles averaged over the open boundary region and extending 10 grid points into the model domain. The hydrostatic sea level difference is approximated by

$$\Delta\eta \simeq \frac{1}{\rho_S|_{z=0}} \int_D^0 [\rho_S(z) - \rho_N(z)] dz, \quad (1)$$

where  $z$  is depth and  $\rho_N$  and  $\rho_S$  are the northern and southern

densities, respectively [Stigebrandt, 1984; Gill, 1982].  $D$  is the level of no motion, here assumed to be at 750 m depth in the Tethys and the Arctic Sea.

The prescribed open boundary depth profiles of temperature  $T_{cp}$  and salinity  $S_{cp}$  for the Arctic and Tethys are chosen to be exponential in form. Only the relative  $T$  and  $S$  distributions are of interest in order to investigate the importance of various external forces. A surface salinity  $S_{cp}|_{(z=0)} = 30$  psu is used for the Arctic profile, and  $S_{cp}|_{(z=0)} = 37$  psu for the Tethys. The salinity and temperature used at 750 m depth are taken to be intermediate between the present-day values and those of global ocean models with Jurassic-like paleogeographies such that  $T_{cp}|_{(z=750)} = 7^\circ$  and  $8^\circ\text{C}$  and  $S_{cp}|_{(z=750)} = 34.5$  and  $35.5$  psu for the Arctic and Tethys, respectively [Kutzbach *et al.*, 1990; Schmidt and Mysak, 1996]. The model results presented here can be regarded as one end-member of the range of possible values of seaway flow because these  $S_{cp}$  and  $T_{cp}$  profiles produce a large but physically possible  $\Delta\eta$ .

### 4.3. Numerical Model Calculations

Two series of model calculations are carried out in order to identify the contributions of the different forces to the circulation. The first series includes the basic spin-up calculation and control calculation (SC0) with all surface and open boundary forces active. In seven other sensitivity tests (SC1-SC5c), successively, a different external force is removed (Table 1). The calculated velocities of a given calculation are then subtracted from the control calculation. The velocity difference in each case gives the contribution from the force removed, when nonlinear terms are negligible [Wang *et al.*, 1994]. The flow is nonlinear in the southwestern part of the seaway owing to the wind stress curl,

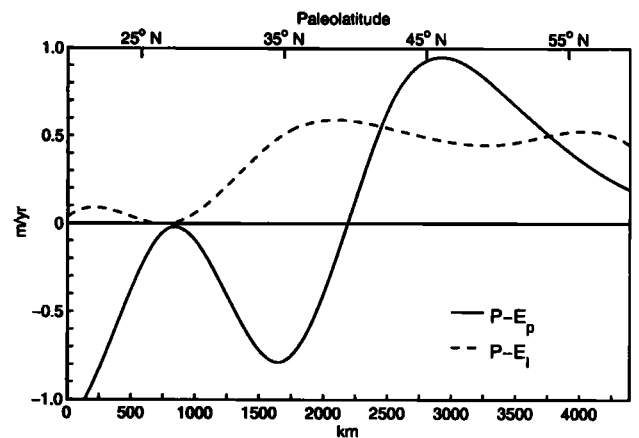


**Figure 4.** Precipitation minus evaporation over sea ( $P - E_p$ ) and over land ( $P - E_l$ ) [Chandler *et al.*, 1992]. A maximum of +1000 mm/yr in the ( $P - E_p$ ) balance occurs over the seaway constriction at 45°N, whereas a minimum of -800 mm/yr is found over the North Sea region. For ( $P - E_l$ ),  $P$  is from the AGCM results, whereas the evapotranspiration  $E_l$  is calculated from land surface temperature and daylight hours [Chandler, 1994]. Almost no negative balance is found over land, in contrast to that over the sea.

**Table 1.** Model Runs, First Series<sup>a</sup>  
Contribution to Circulation From Various Forces.

Run	Parameter Tested	Force Considered <sup>b</sup>
SC0	control calculation	
SC1	no wind	wind
SC2	no rivers	river buoyancy
SC4	no surf. flux	surface buoyancy
SC5	barotropic: $T=15^{\circ}\text{C}$ , $S=33$ psu, fixed	total buoyancy
SC5a	fixed $\Delta\eta$ , otherwise as SC5	local buoyancy
SC5b	$\Delta\eta = 0$	$\Delta\eta$
SC5c	no north OBC	$\Delta\eta$ , inflow/outflow

<sup>a</sup>First series: 180 days integrations following the 10 year spin-up.

<sup>b</sup>Force contributions identified from differences between SC0 and SC1 to SC5.

friction, and density effects, so the method does not give valid results in this area. However, elsewhere in the main part of the seaway, the method gives some physical insights at limited computational expense. The spin-up calculation is started from a state of rest with horizontally homogeneous conditions. After 10 model years, a dynamic steady state is reached. Both the control calculation (SC0) and sensitivity calculations (SC1-SC5c) are subsequently carried out under different forcings for periods of 180 days, starting from the conditions reached at the end of the spin-up. Averages of the last 40 days of the control and sensitivity calculations are used for comparison.

In the second series of model calculations, different boundary conditions are used (Table 2). Results from SBC2, SD7, and SW1 are presented in detail, whereas the other calculations are mentioned where appropriate. In SBC2,  $\Delta\eta$  is set to zero artificially on the boundaries, and in SD7, the water depth is set to be 150 m for all water grid points. In SW1 the windfield of *Moore et al.* [1992] is used. Time integration is carried out over 12 model years from a state of rest with a  $T$  and  $S$  distribution as obtained at the end of the SC0. Averages of the last 40 days are used for presentation.

## 5. Results of Control Calculation (SC0)

The difference of surface elevation between the Arctic and Tethys open boundaries is  $\Delta\eta = 0.5$  m, only slightly different from that derived from OBC forcing. The average surface elevation over the seaway proper slopes downward toward the east. The highest elevations (0.2 m) are in the Goban Spur area of the southwestern part the seaway. The lowest seaway elevations (-0.25 m) are found just east of the North Sea Basin. The surface elevation slope within particular straits is not perpendicular to the strait axis but slopes obliquely across the strait.

### 5.1. Transport Stream Function

The seaway volume transport, expressed as the transport stream function, is constructed from the depth-averaged velocity field. There is an overall southward flow (transport) of 2.7 Sv ( $1 \text{ Sv} = 1 \times 10^6 \text{ m}^3 \text{ s}^{-1}$ ) (Figure 5). The main flow is through the North Sea region because of topographic

**Table 2.** Model Runs, Second Series: Change of Mean Seaway Flow  $\bar{Q}$ , Temperature  $T$  and Salinity  $S$  to Different BC<sup>a</sup>

Run	Parameter Changed	Principal Changes versus SC0
SBC1	$\Delta\eta = 0$	$\bar{Q}$ northward and weak in KS, $T$ increase, $S$ decrease/increase north/south of KS (section 7.1)
SBC2	no open boundary	As SBC1
SW1	alternative wind <sup>b</sup>	$\bar{Q}$ decrease by 13% in KS and most passes through VS, fronts move to Tethys margin, stratification decrease slightly in NSB/CB, PB, SGB
SW2	present wind <sup>c</sup>	$\bar{Q}$ decrease by 19% in KS and all pass through VS, southwest gyre is stronger, stratification decrease in NSB/CB, PB, SGB, 1-4°C increase south of 45°N except in northeast NSB (2°C decrease), 0.5-1.5 psu decrease northwest of SP-LBP
SD1	$1.5H_{\text{control}}$	deeper seaway: $\bar{Q}$ increase as in (2), vertical mixing over sills decrease, stratification increase slightly
SD2	$0.5H_{\text{control}}$	shallower seaway: $\bar{Q}$ decrease as in (2), vertical mixing over sills decrease, stratification decrease slightly
SD3	no VH and ALH	more open to Tethys: 0.5°C, 0.3 psu increase in SGB, PB mixed layer
SD4	$0.3H$ in VS	VS flow restricted: $\bar{Q}$ mostly through FR, RR, 1°-3°C increase east of SP-IBM, <1 psu increase south of 40°N, stratification decrease in SGB, PB, CB
SD5	$0.3H$ in FR-RR	restricted FR, RR flow: $\bar{Q}$ mostly through VS, 0.5°C decrease east of SP-IM, 0.2 psu decrease northeast of IM-AM
SD6	+40 m over seaway	no islands: $\bar{Q}$ increase along central part of seaway, vertical mixing decrease slightly
SD7	uniform $H=150$ m	$\bar{Q}$ increase as in (2), currents trapped along western side of seaway (section 7.2)

<sup>a</sup>Twelve year integration from  $T$  and  $S$  field of the control run (SC0). Abbreviations as in Figure 2 and Notation.

<sup>b</sup>Wind field from *Moore et al.* [1992].

<sup>c</sup>Present-day zonally averaged annual mean windstress.

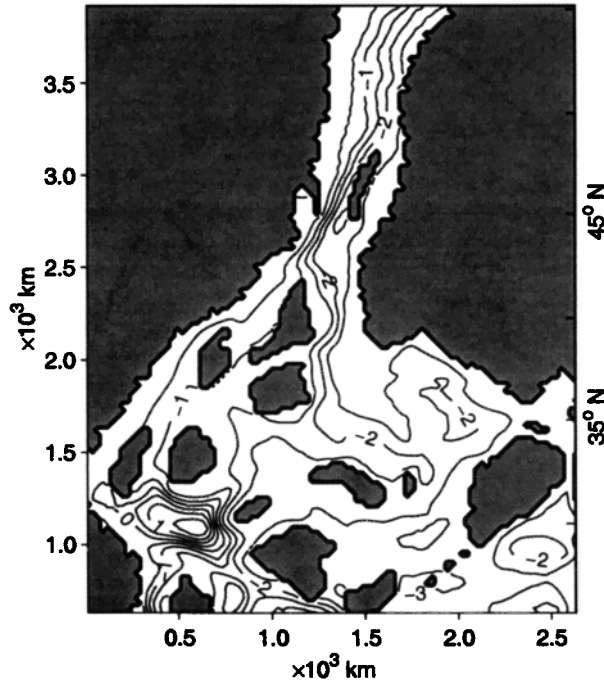


**Figure 5.** Control run transport stream function.  $CI = 0.5$  Sv, where  $1 \text{ Sv} = 10^6 \text{ m}^3 \text{ s}^{-1}$ . The transport is counterclockwise along negative contours (lows). Currents are stronger at closely spaced contours. Note the overall southward transport in the Viking Strait (contours negative) and that the contours lie slightly oblique to individual strait axes.

blocking by sills around the Hebrides platform [Wang *et al.*, 1994]. The stream function contours also illustrate the antisymmetric flow through the straits, which is a result of the coastally trapped currents due to the rotation of Earth [Ohshima, 1994].

The prominent anticyclonic gyre and boundary current in the southwest corner of the seaway is generated by a combination of the wind stress curl in the region and buoyancy forces with associated baroclinic instabilities. The contours of the stream function (currents) are approximately parallel to those of depth and elevation, which illustrates the importance of the variations in relative bathymetry in controlling the local currents. Details of the model flow in sub-basins may not be robust given the uncertainties in paleobathymetry.

The strait volume transports  $Q$  can be approximated by

$$Q = -\frac{g\Delta\eta_s}{fW}A, \quad (2)$$

where  $\Delta\eta_s$  is the strait elevation difference,  $g$  is gravitational acceleration,  $f$  is the coriolis parameter,  $W$  is the width, and  $A$  is the cross-sectional area of the strait [Toulany and Garrett, 1984; Ohshima, 1994]. POM flows for different straits have been compared with the flow derived from (2) (Table 3). Equation (2) is a good approximation that can be used in simplified studies of transcontinental seaways. The

average elevation difference between the Arctic and Tethys Seas is 0.3 m, which gives a southward flow of  $-2.9$  Sv, only slightly larger than the model value of  $-2.7$  Sv.

## 5.2. Temperature and Salinity

The sea surface mixed layer temperatures are in general,  $3^\circ$ – $4^\circ\text{C}$  lower than those expected from climatic  $T_c$  alone because of strong advection of cold waters from the north and the mixing of deeper and surface waters over sills (Figure 6a). The surface temperatures in the southernmost part of the seaway are more closely comparable with those of climatic  $T_c$ . The zonally averaged temperature field shows that deep cold water from the north penetrates into the seaway and that surface waters become gradually warmer toward the south (Figures 6a and 7a). A temperature front is present south of the North Sea ( $\sim 33^\circ\text{N}$ ) and a weak one south of the German and Paris Basins ( $\sim 25^\circ\text{N}$ ).

The average seaway salinity is 33.4 psu south of the Viking Strait, ranging from 33 to 34 psu, which is considerably lower than the average Tethys surface salinity of 35.7 psu (Figure 6b). Deep water of relatively high salinity is advected into the seaway and mixed with surface water of lower salinity over the sill in the Koch Strait (Figure 7b). Low salinity water can be seen penetrating into the South German and Paris Basins, with a salinity front to the Tethys in the south (Figure 7b). The seaway water mass has  $T$  and  $S$  characteristics with Arctic affinity because of strong southward advection driven by the hydrostatic sea level difference.

## 6. Contribution of Different Forces to the Flow

Eight sensitivity tests are carried out to identify the contributions from different forces to the circulation seen in the control run (Table 1). Removing the wind results only in a 5% change in the mean seaway flow (SC1). In SC5, temperature and salinity are set to  $15^\circ\text{C}$  and 33 psu, respectively, over the entire model domain in order to estimate

**Table 3.** POM ( $Q_m$ ) and Analytic ( $Q_s$ ) Strait Flows

Strait	$Q_m$ , Sv	$Q_s$ , <sup>a</sup> Sv	$\Delta\eta_s$ , m	$A$ , $\times 10^6 \text{ m}^2$	$W$ , $\times 10^3 \text{ m}$
Seaway <sup>b</sup>	-2.7	-1.9	0.19	42.6	428
KS <sup>c</sup>	-2.4	-2.1	0.38	11.3	187
VS <sup>c</sup>	-1.7	-0.5	0.07	22.2	321
HPS <sup>c</sup>	-0.2	-0.1	0.03	4.82	134
TBS <sup>c</sup>	-0.7	-0.7	0.08	21.9	321
AHS <sup>c</sup>	-0.1	-0.2	0.01	20.2	187
AMS <sup>c</sup>	-0.3	-0.8	0.04	20.2	161

<sup>a</sup> $Q_s$  from (2) with  $\Delta\eta_s$  across the strait, cross-section area  $A$  and strait width  $W$ .

<sup>b</sup>Flow at  $43^\circ\text{N}$  using the average  $\Delta\eta$  between the Arctic and Tethys.

<sup>c</sup>Strait's defined in Figure 2.

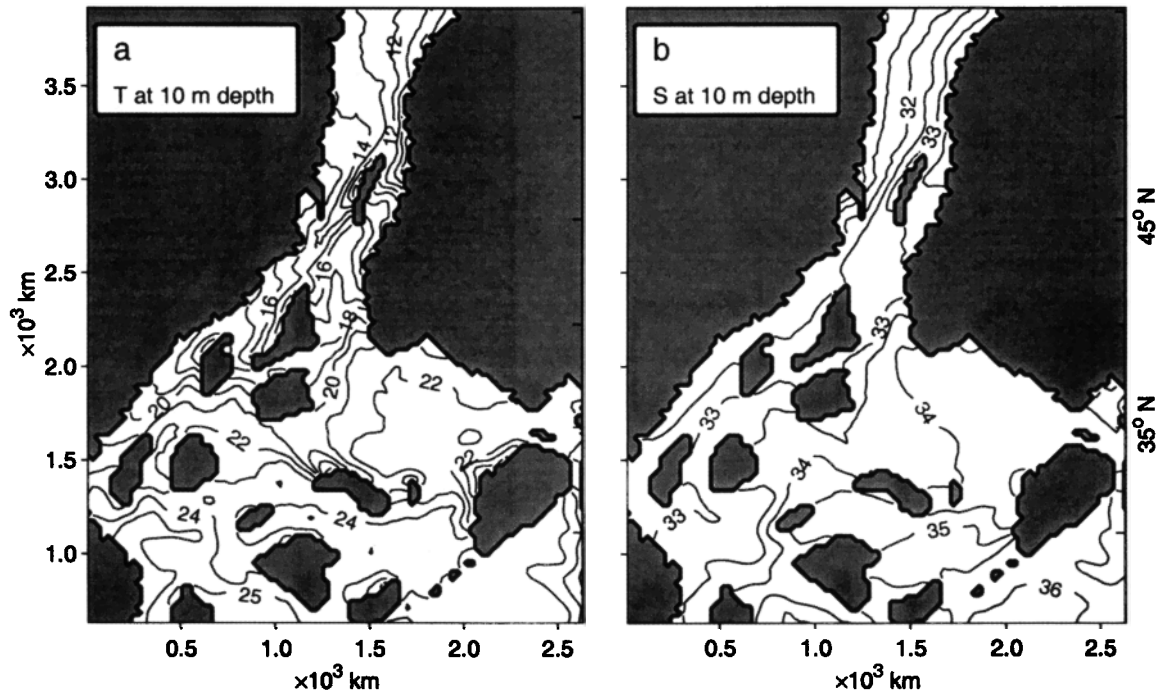


**Figure 6.** Control run (a) temperature and (b) salinity at 10 m water depth.  $CI = 1.0^{\circ}C$  (Figure 6a) and  $CI = 0.5$  psu (Figure 6b). Relatively low values of  $T$  characterize the Koch Strait, whereas  $T$  ranges from  $18^{\circ}$  to  $25^{\circ}C$  south of  $37^{\circ}N$ . Reduced surface salinities occur in the KS and eastern part of the seaway.

the buoyancy effect on water circulation. The salt, heat and river fluxes are also set to zero. The run is equivalent to a barotropic run with no horizontal density differences, in which  $\Delta\eta$  is also zero. The difference between the control run and SC5 gives the baroclinic contribution to the flow (i.e., total buoyancy effects). The buoyancy effects con-

tribute to a southward transport of 2.5 Sv, and almost the entire flow structure of the control run is due to density differences. Run SC5a is carried out as above with uniform  $T$  and  $S$  but now with  $\Delta\eta$  artificially fixed to the value found in the control run, so that the local buoyancy contribution can be identified. The local buoyancy force drives most of the southwest gyre and a slight northward transport of 0.25 Sv through the northern part of the seaway. In run SC5b only the  $\Delta\eta$  parameterization on the open boundary condition is removed.  $\Delta\eta$  is found to contribute to most of the flow in the KS between Greenland and Norway and in the VS in the northern North Sea area.

**7. Influence of  $\Delta\eta$ , Bathymetry and Wind**

The circulation is determined largely by the north-south density gradient, which is a function of the open boundary formulation for the northern and southern oceans. Topographic blocking influences coastal current separation and forces flow through the Viking Strait. The bathymetry and north-south salinity difference and thereby  $\Delta\eta$  are poorly constrained by geological evidence. A series of 11 model runs are therefore carried out to investigate how much the circulation, salinity, and temperature distributions will be altered by modifying the open boundaries, wind forcing, or bathymetry (Table 2).

**7.1. Northern Open Boundary (SBC2)**

An anti-cyclonic circulation develops when there is no hydrostatic sea level difference because the northern boundary

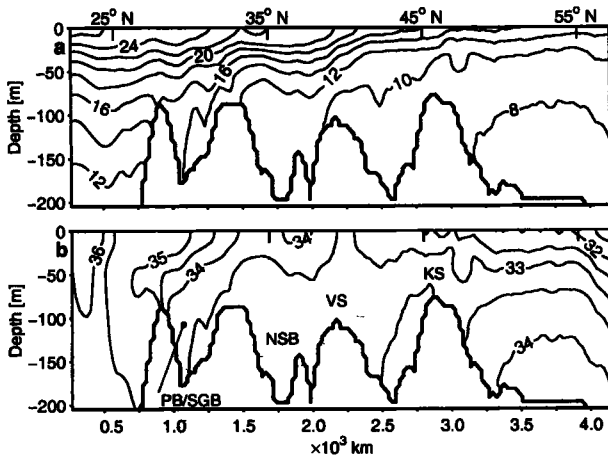


**Figure 7.** Zonally averaged (a) temperature and (b) salinity of the control run ( $CI = 2.0^{\circ}C$  (Figure 7a), 0.25 psu (Figure 7b)).  $T$  and  $S$  are zonally averaged eastward along latitudes from the longitude of the +1000 km grid point (i.e., excluding the southwestern part of the seaway). Bathymetry of water grid points averaged as above and contoured by thick line. Note the low bottom water temperatures within the seaway due to southward advection. Labels are as in Figure 2.

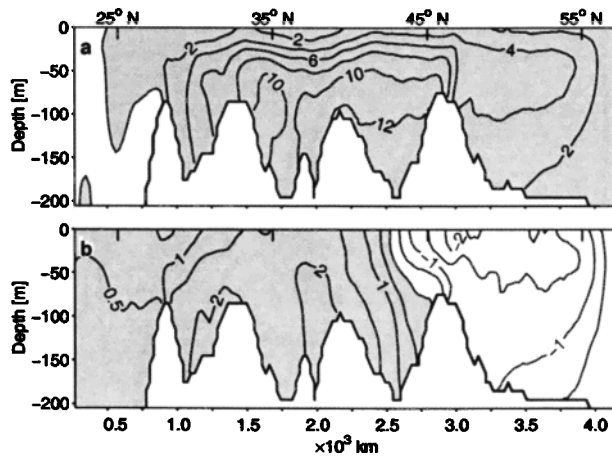


**Figure 8.** Zonally averaged (a) temperature and (b) salinity differences between run SBC2 (closed northern boundary) and the control run (e.g.,  $\Delta T = T_{\text{SBC2}} - T_{\text{SSCO}}$ ).  $\Delta T$  and  $\Delta S$  are zonally averaged as in Figure 7,  $CI = 2^\circ\text{C}$  and  $0.5$  psu (Figures 8a and 8b, respectively).  $S$  and  $T$  are shaded when higher for SBC2. Temperature increases notably below  $-30$  m. Salinity increases south of  $43^\circ\text{N}$  and decreases north of  $43^\circ\text{N}$ .

is closed (not shown) (SBC2, Table 2). Only a weak flow is found in the North Sea region and in the Koch Strait, whereas the anticyclonic gyre in the southwest is twice as strong as in the control run.

Surface temperature and salinity increase by  $1^\circ\text{--}2^\circ\text{C}$  and  $0.5\text{--}1.5$  psu, respectively, over the southern part of the seaway, compared with the control run.  $T$  increases by up to  $4^\circ\text{C}$  around the Shetland platform and northward because there are no strong strait currents and associated turbulent mixing of deeper and shallow water. There is a salinity increase of  $1.5$  psu in the area north of the Irish Massif because relatively high salinity water is advected northward by the anticyclonic flow. Salinities in the KS region decrease by  $1\text{--}2$  psu. Removal of the hydrostatic sea level difference has a dramatic effect at levels below the wind mixed surface layer, as seen in the zonally averaged temperature and salinity fields (Figure 8). Temperatures below  $30$  m water depth increase by  $6^\circ\text{--}12^\circ\text{C}$  south of  $43^\circ\text{N}$ . North of  $45^\circ\text{N}$  the middepth temperature increases by  $4^\circ\text{C}$ . North of  $43^\circ\text{N}$  the salinity is reduced by  $1\text{--}2$  psu, whereas farther south, there is a general salinity increase by  $1.5\text{--}2$  psu below  $30$  m depth.

## 7.2. Changes in Bathymetry (SD7)

The seaway circulation changes significantly relative to the control run when all water grid points have a bathymetry of  $150$  m and no sills are used (Figure 9). Overall, the mean southward flow  $Q$  increases in approximate agreement with (2). No coastal trapped currents are present upstream of previous sills, in agreement with the results of *Ohshima* [1994]. The flow is concentrated along the western side of the seaway because there is no topographic blocking around the Hebrides platform. Trade winds in the eastern side of the

seaway set up a cyclonic gyre in the absence of  $\Delta\eta$ -driven currents in the east.

Surface temperature increases everywhere when a uniform depth is used because turbulent mixing decreases where sills were previously present. A temperature decrease in the western side of the seaway can be attributed to turbulent mixing in the boundary current and southward advection of cold water along its western side. Bottom water temperatures north of  $40^\circ\text{N}$  decrease by  $\sim 1^\circ\text{C}$ , while temperatures in general increase by  $2^\circ\text{--}6^\circ\text{C}$  in the North Sea region because cold water now is advected west of the Shetland Platform (Figure 10a). Temperatures decrease in the bottom waters of the South German and Paris Basins because a reduced sill depth to the Tethys allows deeper cold water to penetrate farther north over the shelf (as in SD3).

Water of low salinity is advected southward primarily along the western side of the seaway. A salinity increase of  $0.5\text{--}1.5$  psu is seen at all levels in the North Sea, South German, and Paris Basins (Figure 10b). Greater water depths over former sill areas reduce turbulent mixing, and bottom waters of relatively higher salinity are not mixed with low-salinity surface waters in the Koch Strait.

Decreasing the water depth only east of the Shetland Platform in run SD4 (Table 2) has a similar effect as described above. Topographic blocking in the Viking Strait increases. Conversely, a decrease in water depth only west of the Shetland Platform blocks the western flow branch, so that virtually all the southward flow passes through the Viking Strait (run SD5, Table 2).

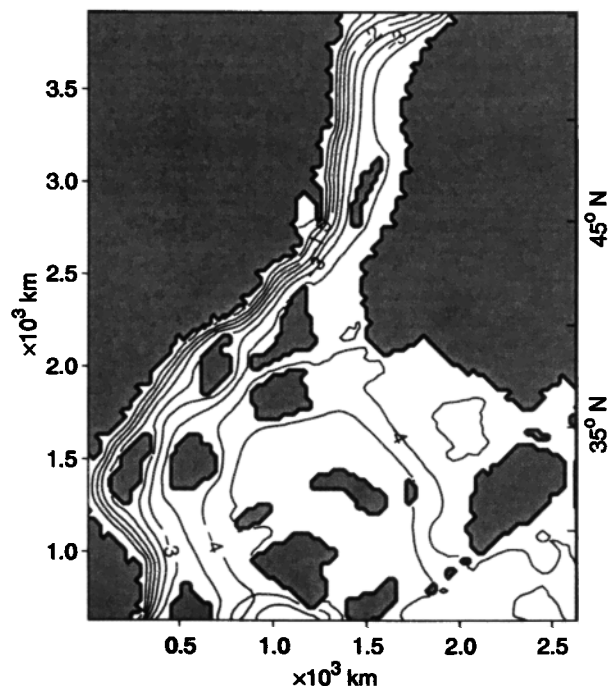


**Figure 9.** Transport streamfunction for a seaway of uniform depth ( $150$  m; run SD7;  $CI = 1$  Sv). A uniform water depth removes all topographic steering and blocking, so that the geostrophic currents follow the western side of the seaway.

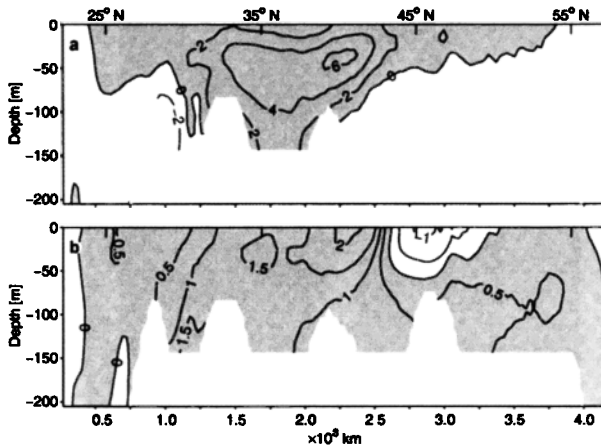


**Figure 10.** Zonally averaged (a) temperature and (b) salinity differences between run SD7 and the control run.  $\Delta T$  and  $\Delta S$  are zonally averaged as in Figure 7 ( $CI = 2.0^\circ\text{C}$  and  $0.5$  psu, respectively). Bathymetry overlap between runs is masked out (white).  $S$  and  $T$  are shaded when higher in SD7. In Figure 10a,  $T$  increases near the surface north of  $34^\circ\text{N}$  because of reduced turbulent mixing over sills.  $T$  also increases in the North Sea basin because no cold water is advected southward in the eastern portion of the seaway. In Figure 10b,  $S$  increases at all levels south of  $43^\circ\text{N}$  and decreases around  $45^\circ\text{N}$ .

**7.3. Different Wind Forcing (SW1)**

The annual mean wind field from Moore *et al.* [1992] is used in SW1 as a test of the possible influence of a different mean wind pattern. The midlatitude westerlies were stronger and located farther south compared to the control run wind field because of the steeper  $T$  gradient in the model. The mean southward flow decreases by  $0.36$  Sv, and most of the southward flow passes through the Viking Strait. The main T/S front moves southward to the northern margin of the Tethys ( $\sim 28^\circ\text{N}$ ). Surface temperatures decrease by  $1^\circ\text{--}2^\circ\text{C}$  over most of the seaway south of  $40^\circ\text{N}$  and along the western side of the seaway. The general decrease in surface temperatures is due to the trade wind stress decrease over the southern part of the seaway, which in turn, leads to a decrease in the northwest advection of warm Tethys water. Upwelling increases along the western side of the seaway at midlatitudes.

**8. Discussion**

Section 7 present results from a series of model calculations exploring the sensitivity to changes in the physical variables that characterize the model. In section 8.1 the results are first summarized and discussed and then synthesized into four robust scenarios with broad Jurassic application. This synthesis is then compared with Early Jurassic (Toarcian) paleontological data.

**8.1. Summary of Model Results**

The numerical calculations corroborate the hypothesis that the Jurassic Laurasian Seaway functioned dynamically as one single strait and that the hydrostatic sea level difference  $\Delta\eta$  between the Tethys Ocean and the Arctic Sea could drive a strong geostrophically controlled current through it. Topographic blocking and steering are important for local details in circulation.  $\Delta\eta$  is the most important control on the overall seaway circulation, temperature and salinity distribution.  $\Delta\eta$  is, in turn, determined by the mean north-south temperature and salinity differences ( $\Delta T_m$  and  $\Delta S_m$ ). Topographic blocking and steering are important for local details in circulation. The calculated local paleocirculation, paleotemperature and paleosalinity details are not robust results given the uncertainty of the bathymetry and surface boundary conditions.

The south-north hydrostatic sea level difference can be obtained approximately from the temperature and salinity differences, a linear equation of state, and (1) (Figure 11). Southward seaway flow results from  $\Delta\eta > 0$  and conversely northward flow results for  $\Delta\eta < 0$ . Only a modest salinity difference is needed for southward flow to be possible during “greenhouse” climatic periods with relatively weak north-south thermal gradients. The salinity difference, how-

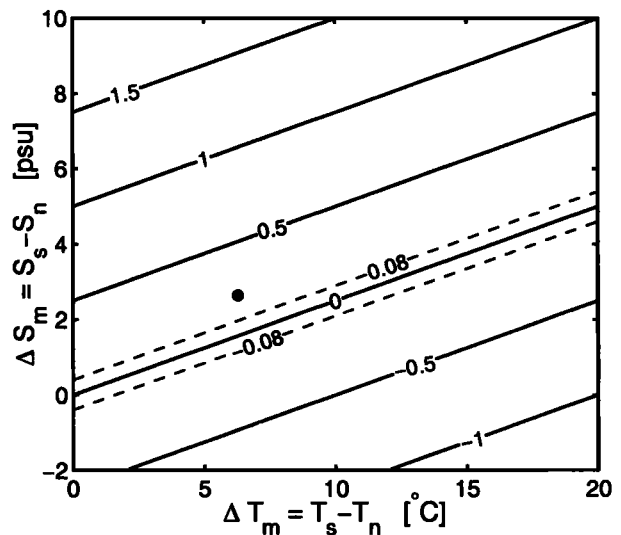


**Figure 11.** Approximate hydrostatic sea level difference  $\Delta\eta$  between the Tethys Ocean and Arctic Sea as a function of south-north temperature difference  $\Delta T_m$  and salinity difference  $\Delta S_m$  (see text for details on calculation).  $\Delta\eta > 0$  corresponds to southward currents and  $CI = 0.5$  m. Solid circle is the approximate average for the control model. Dashed lines bracket the range of  $\Delta\eta$  for which wind-driven flow would be important under present-day annual mean wind stress. The model seaway flow would be northward for  $\Delta S_m = 0$  psu and unchanged  $\Delta T_m$ . The model flow could have been southward or northward for a large range of  $\Delta T_m$ , when  $\Delta S_m > 5$  psu (i.e., when the Arctic has normal marine to slightly reduced salinity). A northward flow results if  $-2 < \Delta S_m < 5$  psu and the temperature gradient is changed to a present-day value.

ever, must be  $>5$  psu for southward flow to develop when  $\Delta T_m > 20^\circ\text{C}$ . The actual salinity difference between the Jurassic Tethys and Arctic Sea is unlikely to have been  $>5$ – $10$  psu because stenohaline normal marine neritic fossils are quite common at high latitudes [Hallam, 1969]. As a consequence, the temperature difference must have been  $<15^\circ\text{C}$  for southward flow to occur.

The POM barotropic flows  $Q_m$  of an idealized 400 km wide and 4000 km long seaway, are calculated for a range of  $\Delta\eta$  values and sill depth configurations (Figure 12). Additionally, a present-day, zonally averaged, annual mean wind stress is applied to give an estimate of a stronger wind influence. The barotropic model flow at  $45^\circ\text{N}$  differs only slightly from the flow derived from (2), which neglects wind. The relatively good correspondence show the limited effect of winds on  $Q_m$ . For  $\Delta\eta = 0$  there is a weak southward flow due to the wind-generated Ekman transport. For the Jurassic wind field, there would be a weak northward flow. The present-day North Atlantic annual mean wind stress ( $\tau_x \sim 0.1 \text{ N m}^{-2}$ ) can set up a flow that corresponds to the flow driven by  $\Delta\eta = -0.08 \text{ m}$  (Figures 11 and 12). Removing the wind from the control run (SC0) only results in a 5% change in the mean seaway flow (section 6). The wind-driven flow was therefore of limited importance for the mean flow, salinity, and temperature of the narrow Jurassic Laurasian Seaway if sill depths or mean seaway depth were  $> 30 \text{ m}$ .

Frictional forces and seaway depth start to dominate the flow magnitude, when mean sill or seaway depths are shallow, as can be seen from the lack of sensitivity to  $\Delta\eta$  when sill depth is less than  $\sim 30 \text{ m}$  (Figure 12). Tidal amplification

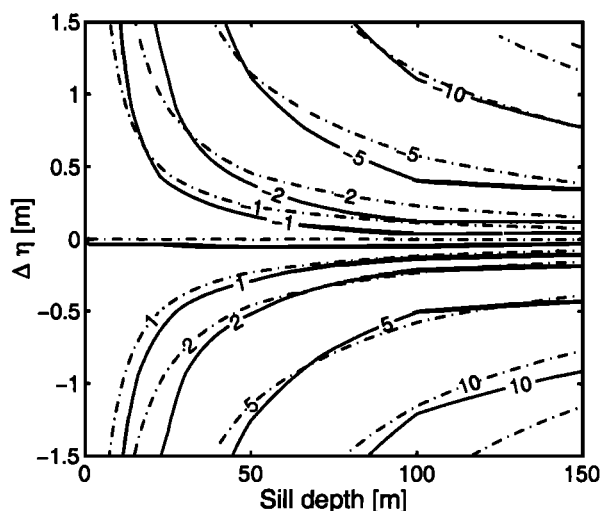


**Figure 12.** POM barotropic flow ( $Q_m$  in Sv, solid lines) at  $45^\circ\text{N}$  for an idealized straight-channel seaway of 400 km width, 3500 km length, and 150 m mean shelf depth, as a function of hydrostatic sea level difference  $\Delta\eta$  and sill depth at  $45^\circ\text{N}$  [Bjerrum, 1999].  $CI = 1 \text{ Sv}$  and is positive for northward flow. Equation (2), where wind is neglected, is shown with dash-dotted lines. For shallow sills,  $Q_m$  is mostly dependent on sill depth, whereas for larger depths,  $\Delta\eta$  is very important.

and the resulting residual currents will be very important for the mean flow when frictional forces dominate. Including tides in the present model therefore would only change the flow slightly in the shallow grid points of the model (30–50 m) [Bjerrum, 1999].

The relative bathymetric differences in the seaway are important in controlling the local current details and the principal route of the main  $\Delta\eta$ -driven current. Only the larger current features are therefore robust results with paleoceanographic implications. Most of the flow leaving a basin with more than one exit will follow the deepest strait (run SD4 versus SD5). The regional wind pattern likewise has an influence on which course the main southward flow will follow. For stronger midlatitude westerly winds most or all of the southward flow is through the Viking Strait area (runs SW1 and SW2).

The wind field used in the control run is very different from that calculated by Moore *et al.* [1992], presumably because they used a diffusive mixed layer ocean in contrast to the fixed sea surface temperatures used by Chandler *et al.* [1992]. The robust results of the present model are only weakly influenced by the fixed sea surface temperatures of the AGCM since the present results primarily depend on the salinity and temperature imposed on the OBC north and south of the seaway. Seaway advection of  $T$  and  $S$  due to the  $\Delta\eta$ -driven flow is more important, as can be seen from the sensitivity calculations (Figures 8 and 10).

Four robust end-member scenarios with general Jurassic implications can be synthesized from the control and sensitivity runs and the discussion (Figures 13a–13d). For  $\Delta\eta > 0$ , overall southward flow predominates and relatively cool water of low salinity is advected into the European region (runs SC0, SW1, SW2, and SD1–SD9). Because of the uncertainties in paleogeography and lithology west of Jurassic Britain, two alternatives are likely, depending on whether water depth or cross-sectional area were greater in the Viking Strait or west of the Shetland Platform (Figures 13a and b; run SD4, SD5, SD7). The flow shown in Figure 13b could also be due to strong midlatitude westerlies (runs SW1 and SW2). For  $\Delta\eta \leq 0$  the main  $T - S$  front would have been located at or north of the main seaway constriction, and water with Tethys  $T$  and  $S$  characteristics would have dominated Europe for both topographic alternatives (Figures 13c and 13d) (runs SBC1 and SBC2).

## 8.2. Geological Discussion

Each of the four end-member scenarios described above would have influenced the marine paleoecological system through the effects on the regional paleohydrosphere and its climate system. Observations from the geological record can be interpreted in light of the model results. For the present purposes the discussion is concerned with regions north of France and Germany where a survey is presented for the Early Jurassic. This survey points to possible ways of testing the present results when more longitudinal data transects

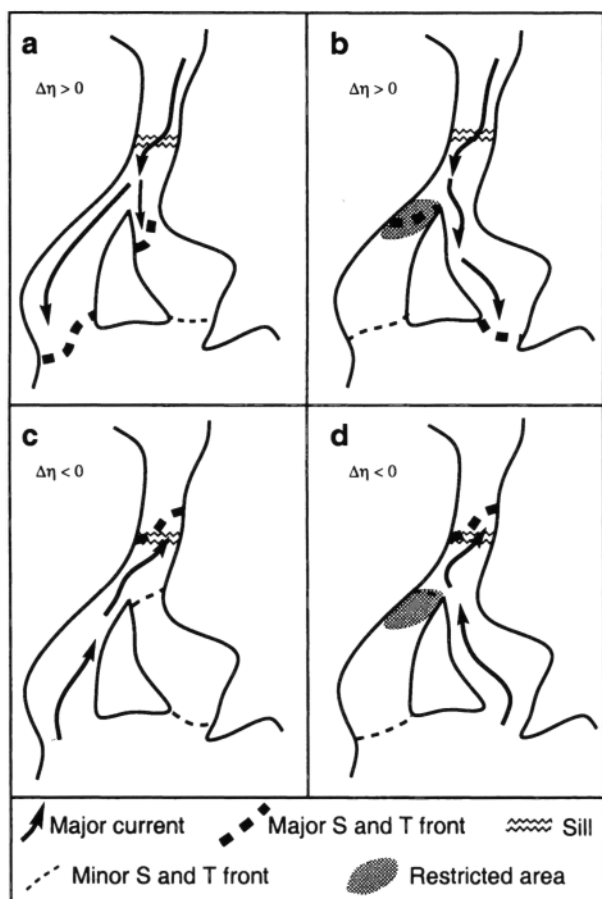


**Figure 13.** Four simplified end-member scenarios (a-d), indicating principal flow routes and the positions of *T/S* water mass fronts. (a) Tethys water denser than Arctic ( $\Delta\eta > 0$ ) and straits west of Shetland Platform (wSP) less restricted than the Viking Strait. (b)  $\Delta\eta > 0$  but with wSP the more restricted and/or with strong midlatitude westerlies. (c) Arctic water denser than that of Tethys ( $\Delta\eta \leq 0$ ) and wSP less restricted. (d)  $\Delta\eta \leq 0$  and the wSP more restricted than the Viking Strait area.

with biostratigraphic subzone resolution become available. In the following, abbreviations in brackets refer to those on Figure 2.

Presence of marine biogenic carbonate sediments is believed to reflect relatively high temperatures, normal marine salinity and oligotrophy of the photic zone. The European Jurassic shows a latitudinal transition from predominantly carbonates in the south to predominantly siliciclastic sediments north and east of the Hebrides (HP). From east to west the transition zone can be relatively sinuous, over several degrees of latitude, and probably reflects the marine circulation.

In the Early Jurassic, carbonate-rich deposits dominated or were significant southwest of a boundary zone extending from the Irish Massif (IM) southeastward to the southern margins of the Bohemian Massif (BM). The contrast is reflected by the Lower Jurassic limestones of the Lusitanian (~IBM) and Paris Basins (PB) south and west of the dark

shales of the Lower Jurassic Black Jura of southern Germany (SGB). Hermatypic corals reached northward to the Hebrides in the Hettangian. The carbonate-siliciclastic transition may be seen in Britain (northwest of LBP). These distributions imply north-south marine connections both east and west of Britain (SP-IM-LBP) and marine circulation as in scenario B (Figure 13b). Arctic waters flow southward east of Britain, and warmer water flow northward west of Britain as a result of wind-driven circulation and/or constriction near the Hebrides (compare SD4 and SD5 and SW1). Various climate-sensitive sedimentary facies, clay mineralogy, and pollen data suggest that the European Late Pliensbachian and Toarcian were climatically more temperate periods compared with those before and after, as would be expected when sea surface temperatures were reduced during southward flow as in scenario B [Delfaud, 1983].

For purposes of comparison with ocean circulation model calculations, fossil distribution patterns are intriguing. Ammonites show a strong bioprovincial endemism in the Mesozoic since the late Early Jurassic and reveal latitudinal ranges almost certainly related to climatic factors and marine circulation patterns [Hallam, 1969; Page, 1996]. The changes of bioprovincial boundaries with time have implications for the interpretation of the overall marine circulation. For many ammonites, habitats ranged from relatively shallow shelf waters at birth and at death to deeper water during growth [Callomon, 1985]. The migrational ranges during the life cycle could have been on a scale of 1000 km. Other ammonites were probably inhabiting the oceans and strayed into shallow waters in pursuit of food in favorable surface waters or by postmortal drift (e.g., *Phylloceras*, *Lytoceras*).

Evidence of ammonite distributions north of the Tethys is good in southern England (southwest of LBP) and southward. Farther north, well-preserved Early Toarcian faunas are recorded in northeast England (CB), in the Hebrides (east of HP), in central east Greenland west of KS, and on Spitsbergen (in the Arctic Sea) [Ershova and Repin, 1983; Bäckström and Nagy, 1985; Howarth, 1992].

The Laurasian Seaway was to varying degrees populated by five major long-ranging groups where *Pseudolioceras* is the earliest truly boreal genus found in the Jurassic and occurring throughout the Arctic, eastern Siberia, and Alaska [Dagis, 1974]. *Pseudolioceras* is commonly the dominant or sole component of the ammonite fauna north of central east Greenland. At discrete times, *Pseudolioceras* spread southward into Europe as far as the southern Paris Basin (PB) but as a rapidly diminishing component of the faunas. This indicates direct open marine connections with the Arctic through the VS in the east. There is further a marked decrease southwestward, so that the genus becomes rare in southern England (west of LBP). This coincides with the carbonate boundary zone, where fine-grained, dark, distal mudstones pass into condensed, offshore marls and limestones in southern England. Early Toarcian members of Tethys groups (Harpoceratinae and Hildoceratinae)

are strongly represented as far as northeast England but occur only rarely in central east Greenland (*Hildaites*), G. Dam coll.) and on Spitsbergen (as "*Pseudogrammoceras*" of *Bäckström and Nagy* [1985]), whereas the Tethyan Phymatoceratidae have not been found north of northeast England (CB). These observations suggest that there was a transition in England from southward flowing cold waters in the northeast to warmer waters in the southwest (Figure 13b). The periods of strongest southward excursion of boreal *Pseudolioceras* approximately coincided and alternated with the most frequent northerly excursions of the archetypically Tethyan *Liostraca*, (*Phylloceras* and *Lytoceras* [Dean, 1954]). Both the durations of southerly excursions of *Pseudolioceras* and the intervals between them were highly variable with wide changes of distribution occurring very rapidly [Dean, 1954; Howarth, 1992]. On the shortest timescale the genus can be concentrated into a single bed spanning a fraction of a standard ammonite subzone ( $\sim 10^4$  years). Sporadic appearances can extend over one or several subzones ( $\sim 10^6$  years), and gaps can be of similar magnitudes. These rapid fluctuations in ammonite distributions could be interpreted as the result of relatively fast changes in the north-south density differences and hence seaway currents.

Lithofacies and faunal latitudinal changes in Middle and Late Jurassic times suggest, despite differences in seaway paleogeography, that seaway currents may have reversed owing to changes in salinity at high latitudes in the open ocean. The Middle and Late Jurassic will be treated in more detail in a future study. Overall, the lithofacies and paleobiogeographic provinces of the Jurassic suggest that southward seaway currents dominated in the Toarcian, Early Callovian, latest Callovian to Early Oxfordian, late Middle and Late Oxfordian, and in the Kimmeridgian. In intervening periods the currents flowed northward or were blocked by very shallow sills or land as in much of the Middle Jurassic.

Southward currents correspond with periods where high-latitude ocean salinities were reduced which possibly prevented northern high-latitude convection [cf. *Shaffer and Bendtsen*, 1994; *Schmidt and Mysak*, 1996]. It is therefore proposed that deepwater formation might have been occurring in the Tethys and/or at southern high latitude [Schmidt and Mysak, 1996; Bjerrum, 1999]. The possible relation between the global thermohaline circulation and seaway flow directions require further study and imply that geological data from ancient meridional seaways perhaps can be used to elucidate the ancient state of the thermohaline circulation [Bjerrum, 1999].

## 9. Summary and Perspective

The Princeton Ocean Model is used to advance our understanding of the paleoceanographic processes in transcontinental seaways. The global ocean is found to have a profound influence on seaway dynamics. Model calculations show that the Jurassic transcontinental Laurasian Seaway

can be regarded as one single strait for modeling purposes, despite its complex paleogeography. Hydrostatic sea level differences between the Tethys Ocean and the Arctic Sea could have driven a strong current through the seaway. Bathymetric variation was important for local circulation in subbasins, whereas the minimum sill depth exerted the dominant control of the net magnitude of the transcontinental seaway flow. Bathymetric uncertainty dictates that calculated current details of scales less than  $\sim 200$  km are not significant.

North-south density differences and hence hydrostatic sea level differences have a large impact on seaway salinity and temperature. When Tethyan waters are the denser (low hydrostatic sea level), the seaway flow is southward, giving the waters in the seaway Arctic characteristics. Conversely, when the Arctic waters are the denser, the seaway waters have Tethyan characteristics. Changes in wind patterns or strengths have only little impact on the net southward or northward seaway flow.

Net seaway current directions in the Jurassic can be inferred from latitudinal shifts in paleobiogeographic provinces, in particular, of ammonites. Arctic influences on seaway waters are indicated by faunal dominance and southward spread of boreal ammonites and cooler climatic conditions inferred from palynology and clay mineralogy. Conversely, Tethys-influenced seaway waters may be inferred from sub-Mediterranean faunal influences and indicators of warmer water/climate. An increased understanding of the Jurassic ocean-climate system should be possible if the model calculations are tested within the framework of high-resolution paleobiogeographical and geochemical studies. This would result in a better understanding of the anoxic/dysoxic events that apparently were associated with the hypothesized southward flow in the Toarcian and in the Kimmeridgian.

## Notation

$x, y, z$	east, north, and upward coordinate axis (0,0,0 in southwest model corner).
$f(y)$	Coriolis parameter, $s^{-1}$ .
$\rho(x, y, x)$	density, $kg\ m^{-3}$ .
$H(x, y)$	water depth, m.
$P - E_p(x, y)$	precipitation minus open-water evaporation, $m\ s^{-1}$ .
$P - E_l(x, y)$	precipitation minus evapotranspiration over land, $m\ s^{-1}$ .
$T(x, y, z)$	temperature, $^{\circ}C$ .
$T_c(x, y)$	sea surface climatic temperature, $^{\circ}C$ .
$T_{cp}(z)$	open-boundary temperature, $^{\circ}C$ .
$S(x, y, z)$	salinity, psu (approximately $\%_{00}$ ).
$S_{cp}(z)$	open-boundary salinity, psu.
$\Delta\eta$	hydrostatic sea level difference, m.
$Q$	strait volume transport, $m\ s^{-1}$ .
$z_r(H)$	roughness length scale, m.

$\Delta T_m$  mean south-north  $T$  difference, °C.

$\Delta S_m$  mean south-north  $S$  difference, psu.

**Acknowledgments.** We gratefully acknowledge Mark Chandler for supplying the AGCM data files and thank Jørgen Bendtsen, Gary Shaffer, and Steve Hesselbo for thoughtful and stimulating

discussions. The manuscript has benefited by comments from J. Bendtsen and reviews by P. Jewell and two anonymous reviewers. The research was funded by a University of Copenhagen stipend to C. J. Bjerrum and a grant from the Danish Natural Science Research Council (SNF) to F. Surlyk. Supercomputer time was funded by the SNF. Danish Center for Earth System Science (DCESS) funded the final work.

## References

- Ager, D. V., The Jurassic world ocean, in *Jurassic Northern North Sea Symposium*, edited by K. Finstad and R. C. Selley, pp. 1–43, Nor. Petrol. Soc., Stavanger, 1975.
- Bäckström, S. A., and J. Nagy, Depositional history and fauna of a Jurassic phosphorite conglomerate (the Bretnskardhaugen Bed) in Spitsbergen, *Skr. Nor. Polarinst.*, 185, 44 p., 1985.
- Bjerrum, C., Numerical paleoceanography of a Jurassic narrow meridional seaway: Transcontinental currents and global ocean feedbacks, Ph.D. thesis, Univ. of Copenhagen, Copenhagen, Denmark, 1999.
- Blumberg, A. F., and G. L. Mellor, Diagnostic and prognostic numerical circulation studies of the South Atlantic Bight, *J. Geophys. Res.*, 88, 4579–4592, 1983.
- Blumberg, A. F., and G. L. Mellor, A description of a three-dimensional coastal ocean circulation model, in *Three-Dimensional Coastal Ocean Models*, *Coastal Estuarine Sci. Ser.*, vol. 4, edited by N. Heaps, pp. 1–16, AGU, Washington, D. C., 1987.
- Bradshaw, M. J., et al., Jurassic, in *Atlas of Paleogeography and Lithofacies*, *Mem. Geol. Soc.*, vol. 13, edited by J. C. W. Cope, J. K. Ingram, and P. F. Rawson, pp. 107–129, Geol. Soc., London, 1992.
- Bretschneider, C. L., Wave generation by wind, deep and shallow water, in *Estuary and Coastline Hydrodynamics*, *Eng. Soc. Monogr.*, edited by A. T. Ippen, pp. 133–198, McGraw-Hill, New York, 1966.
- Buchem, F. S. P. V., and I. N. McCave, Cyclic sedimentation patterns in Lower Lias mudstones of Yorkshire (GB), *Terra Nova*, 1, 461–467, 1989.
- Cai, W., and S. J. Godfrey, Surface heat flux parameterization and the variability of the thermohaline circulation, *J. Geophys. Res.*, 100, 10679–10692, 1995.
- Callomon, J. H., Marine boreal Bathonian fossils from the northern North Sea and their palaeogeographical significance, *Proc. Geol. Assoc.*, 90, 163–169, 1979.
- Callomon, J. H., The evolution of the Jurassic ammonite family Cardioceratidae, *Spec. Pap. Palaeontol.*, 33, 49–90, 1985.
- Chandler, M. A., Description of modern and Pangean deserts. Evaluation of GCM hydrological diagnostics for paleoclimate studies, in *Pangea: Paleoclimate, Tectonics, and Sedimentation During Accretion, Zenith, and Breakup of a Supercontinent*, edited by G. D. Klein, *Spec. Pap. Geol. Soc. Am.*, 288, 117–138, 1994.
- Chandler, M. A., D. Rind, and R. Ruedy, Pangean climate during the Early Jurassic. GCM simulations and the sedimentary record of paleoclimate, *Geological Society of America Bulletin*, 104, 543–559, 1992.
- Dagis, A. A., *Toarskie ammonity (Hildoceratidae) Severa Sibiri [Toarcian ammonites (Hildoceratidae) of the North Siberia]*, Nauka, Moscow, 1974.
- Dean, W. T., Notes on part of the Upper Lias succession at Blea Wyke, Yorkshire, *Proc. Yorkshire Geol. Soc.*, 29, 161–182, 1954.
- Delfaud, J., Les paléoclimats du Jurassique en Europe occidentale, *Bull. Inst. Geol. Bassin Aquitaine*, 34, 121–135, 1983.
- Diem, B., Analytical method for estimating palaeowave climate and water depth from wave ripple marks, *Sedimentology*, 32, 705–720, 1984.
- Dreyer, T., Significance of tidal cyclicity for modelling of reservoir heterogeneities in the lower Jurassic Tilje Formation, mid-Norwegian shelf, *Nor. Geol. Tidsskr.*, 72, 159–170, 1992.
- Erickson, M. C., and R. L. Slingerland, Numerical simulation of tidal and wind-driven circulation in the Cretaceous Interior Seaway of North America, *Geol. Soc. Am. Bull.*, 102, 1499–1516, 1990.
- Ershova, E. S., and Y. S. Repin, Toarskie i aalen-skie ammonity archipelaga Shpitsbergen, in *Geologiya Shpitsbergena*, edited by A. A. Krasilyshchikov and V. A. Basov, pp. 150–170, Minist. Geol. SSSR, Leningrad, Russia, 1983.
- Gill, A. E., *Atmosphere-Ocean Dynamics*, Academic, San Diego, Calif., 1982.
- Hallam, A., Faunal realms and facies in the Jurassic, *Palaeontology*, 12, 1–18, 1969.
- Hallam, A., Continental humid and arid zones during the Jurassic and Cretaceous, *Palaeogeogr. Palaeoclimatol. Palaeoecol.*, 47, 195–223, 1984.
- Hallam, A., A reevaluation of Jurassic eustasy in the light of new data and the revised Exxon curve, in *Sea-Level Changes: An Integrated Approach*, edited by C. K. Wilgus et al., *Spec. Pub. SEPM*, 42, 261–274, 1988.
- Hallam, A., Jurassic climates as inferred from the sedimentary and fossil record, *Philos. Trans. R. Soc. London. Ser. B*, 341, 287–296, 1993.
- Hallam, A., and P. B. Wignall, *Mass Extinctions and Their Aftermath*, Oxford Univ. Press, New York, 1997.
- Hay, W., Paleoclimatology of marine organic-carbon-rich sediments, in *Paleogeography, Paleoclimate, and Source Rocks*, edited by A. Y. Huc, *AAPG Stud. Geol.*, 40, 21–59, 1995.
- Hesselbo, S., D. Gröcke, H. Jenkyns, C. Bjerrum, P. Farrimond, H. M. Bell, and O. Green, Massive dissociation of gas hydrate during a Jurassic oceanic anoxic event, *Nature*, 406, 392–395, 2000.
- Holland, H. D., *The Chemistry of the Atmosphere and Oceans*, John Wiley, New York, 1978.
- Holloway, P. E., and B. Barnes, A numerical investigation into the bottom boundary layer flow and vertical structure of internal waves on a continental slope, *Cont. Shelf Res.*, 18, 31–65, 1998.
- Howarth, M. K., *The Ammonite Family Hildoceratidae in the Lower Jurassic of Britain*, *Monogr. Palaeontogr. Soc., Palaeontogr. Soc.*, London, 1992.
- Jenkyns, H. C., The Early Toarcian (Jurassic) anoxic event: Stratigraphic, sedimentary and geochemical evidence, *Am. J. Sci.*, 288, 101–151, 1988.
- Jewell, P. W., Circulation, salinity, and dissolved oxygen in the Cretaceous North American seaway, *American Journal of Science*, 296, 1093–1125, 1996.
- Kutzbach, J. E., P. J. Guetter, and W. M. Washington, Simulated circulation of an idealized ocean for Pangean time, *Paleoceanography*, 5, 299–317, 1990.
- Mellor, G., *Users guide for a three-dimensional primitive equation, numerical ocean model*, Program in Atmos. and Oceanic Sci., Princeton Univ., Princeton, N.J., 1998.
- Miller, R. G., A paleoceanographic approach to the Kimmeridge Clay Formation, in *Deposition of Organic Facies*, edited by A. Y. Huc, *AAPG Stud. Geol.*, 30, 13–26, 1990.
- Moore, G. T., D. N. Hayashida, C. A. Roos, and S. R. Jacobson, The paleoclimate of the Kimmeridgian/Tithonian (Late Jurassic) world, I., Results using a general circulation model, *Palaeogeogr. Palaeoclimatol. Palaeoecol.*, 93, 113–150, 1992.
- O'Brien, N. R., Significance of lamination in the Toarcian (Lower Jurassic) shales from Yorkshire, Great Britain, *Sediment. Geol.*, 67, 25–34, 1990.
- Oey, L.-Y., Simulation of mesoscale variability in the Gulf of Mexico: sensitivity studies, comparison with observations, and trapped wave propagation, *J. of Phys. Oceanogr.*, 26, 145–175, 1996.
- Oey, L.-Y., Subtidal energetics in the Faroe-Shetland Channel. Coarse-grid model experiments, *J. Geophys. Res.*, 103, 12689–12708, 1998.
- Oey, L.-Y., and P. Chen, A model simulation of circulation in the northeast Atlantic shelves and seas, *J. Geophys. Res.*, 97, 20087–20115, 1992.
- Ohshima, K. I., The flow system in the Japan Sea caused by a sea level difference through shal-

- low straits, *J. Geophys Res*, **99**, 9925–9940, 1994.
- Page, K. N., Mesozoic ammonoids in space and time, in *Ammonoid Paleobiology*, edited by N. Landman, K. Tanabe, and R. A. Davis, *Top. Geobiol.*, **13**, pp. 755–793, 1996.
- Paterson, D. M., and K. S. Black, Water flow, sediment dynamics and benthic biology, *Adv. Ecol. Res.*, **29**, 155–193, 1999.
- Picard, S., et al.,  $\delta^{18}\text{O}$  values of coexisting brachiopods and fish. Temperature differences and estimates of paleo-water depths, *Geology*, **26**, 975–978, 1998.
- Prauss, M., B. Ligouis, and H. Luterbacher, Organic matter and palynomorphs in the 'Posidonienschiefer' (Toarcian, Lower Jurassic) of southern Germany, in *Modern and Ancient Continental Shelf Anoxia*, edited by R. V. Tyson and T. H. Pearson, *Geol. Soc. Special Publ.*, **58**, pp. 335–351, 1991.
- Rees, P. M., A. M. Ziegler, and P. J. Valdes, Jurassic phytogeography and climates: New data and model comparisons, in *Warm Climates in Earth History*, edited by B. T. Huber, K. G. MacLeod, and S. L. Wing, pp. 297–318, Cambridge Univ. Press, New York, 2000.
- Röhl, H.-J., A. Schmid-Röhl, W. Oschmann, A. Frimmel, and L. Schwark, The Posidonia Shale (Lower Toarcian) of SW-Germany: An oxygen-depleted ecosystem controlled by sea level and palaeoclimate, *Palaeogeogr. Palaeoclimatol. Palaeoecol.*, **165**, 27–52, 2001.
- Sælen, G., R. V. Tyson, M. R. Talbot, and N. Telnæs, Evidence of recycling of isotopically light  $\text{CO}_2(\text{aq})$  in stratified black shale basins: Contrasts between the Whitby Mudstone and Kimmeridge Clay Formations, United Kingdom, *Geology*, **26**, 747–750, 1998.
- Schieber, J., Microbial mats in terrigenous clastics: The challenge of identification in the rock record, *Palaios*, **14**, 3–12, 1999.
- Schmidt, G. A., and L. A. Mysak, Can increased poleward oceanic heat flux explain the warm Cretaceous climate?, *Paleoceanography*, **11**, 579–593, 1996.
- Schouten, S., H. E. V. Kaam-Peters, W. I. C. Rijpstra, M. Schoell, and J. S. S. Damste, Effects of an oceanic anoxic event on the stable carbon isotopic composition of Early Toarcian carbon, *Am. J. Sci.*, **300**, 1–22, 2000.
- Shaffer, G., and J. Bendtsen, Role of the Bering Strait in controlling North Atlantic Ocean circulation and climate, *Nature*, **367**, 354–357, 1994.
- Silva, A. M. D., C. C. Young, and S. Levitus, *NOAA Atlas NESDIS, 9, Atlas of surface marine data 1994, vol. 4*, 1994.
- Slingerland, R. L., L. R. Kump, M. A. Arthur, P. J. Fawcett, B. Sageman, and E. J. Barron, Estuarine circulation in the Turonian Western Interior Seaway of North America, *Geol. Soc. Am. Bull.*, **108**, 941–952, 1996.
- Smith, A. G., D. G. Smith, and B. M. Funnell, *Atlas of Mesozoic and Cenozoic Coastlines*, Cambridge Univ. Press, New York, 1994.
- Stigebrandt, A., The North Pacific: A global-scale estuary, *J. of Phys. Oceanogr.*, **14**, 464–470, 1984.
- Toulany, B., and C. J. R. Garrett, Geostrophic control of fluctuating flow through straits, *J. of Phys. Oceanogr.*, **14**, 649–655, 1984.
- Valdes, P. J., and B. W. Sellwood, A palaeoclimatic model for the Kimmeridgian, *Palaeogeogr. Palaeoclimatol. Palaeoecol.*, **95**, 47–72, 1992.
- Wang, J., L. A. Mysak, and R. G. Ingram, A three-dimensional numerical simulation of Hudson Bay summer ocean circulation: Topographic gyres, separation, and coastal jets, *J. of Phys. Oceanogr.*, **24**, 2496–2514, 1994.
- Whitehead, J. A., Topographic control of oceanic flows in deep passages and straits, *Rev. Geophys.*, **36**, 423–440, 1998.
- Ziegler, P. A., Evolution of the Arctic-North Atlantic and the western Tethys, *AAPG Mem.*, **43**, p. 198 pp., 1988.
- Ziegler, P. A., *Geological Atlas of Western and Central Europe*, Shell Int. Petrol. Maatschappij B. V., The Hague, Netherlands, 1990.

C. J. Bjerrum, Danish Center for Earth System Science, Niels Bohr Institute for Astronomy, Physics and Geophysics, University of Copenhagen, Juliane Maries Vej 30, DK-2100 Copenhagen Ø, Denmark. (cjb@dcess.ku.dk).

J. H. Callomon, Chemistry Department, University College London, 20 Gordon Street, London WC1H 0AJ, England, UK.

Rudy L. Slingerland, Department of Geosciences, Pennsylvania State University, University Park, PA 16802.

F. Surlyk, Geological Institute, University of Copenhagen, Øster Voldgade 10, DK-1350 Copenhagen K, Denmark.

(Received February 15, 2000;

revised February 22, 2001;

accepted March 12, 2001.)